Aerodynamic Response of a Hovering Rotor to Ramp Changes in Pitch Input

Karthikeyan Duraisamy
Lecturer

Richard E Brown
Mechan Chair of Engineering

Department of Aerospace Engineering
University of Glasgow
Glasgow G12 8QQ
United Kingdom

Abstract

Under transient conditions, a helicopter rotor generates a complex, time-dependent pattern of shed and trailed vorticity in its wake that has profound effects on its loading. To examine these effects, the response of a two-bladed hovering rotor to a ramp change in collective pitch is investigated using three different computational approaches. Solutions obtained using a Compressible Reynolds Averaged Navier–Stokes approach are compared to results obtained from lifting-line theory coupled to an Eulerian Vorticity Transport Model, and from a simple single-state dynamic inflow model. The different numerical approaches yield very similar predictions of the thrust response of the rotor to ramp changes in collective pitch, as long as the ramp rates are small. This suggests that the basic underlying flow physics is properly represented by all the approaches. For more rapid ramp rates, an additional delay in the aerodynamic response of the rotor, that is related to the finite extent of the wake during its early history, is predicted by the Navier–Stokes and Vorticity Transport approaches. Even though the evolution of the wake of the rotor is strongly three dimensional and highly unsteady, the predictions of the Navier–Stokes and lifting-line models agree very closely as long as the blades of the rotor do not stall. In the pre-stall regime, a quasi two-dimensional representation of the blade aerodynamics thus appears adequate for predicting the performance of such systems even under highly transient conditions. When flow separation occurs, the resulting three dimensionality of the blade aerodynamics forces the predictions of the Navier–Stokes and lifting-line approaches to diverge, however. The characterization of the wake interactions and stall propagation mechanisms that are presented in this study offers some insight into the fundamental fluid dynamic mechanisms that govern the transient aerodynamic response of a rotor to control inputs, and provides some quantification of the limits of applicability of some popular current approaches to rotor aerodynamic analysis.

Notation

ψ	Blade azimuth
ψ_o	Blade azimuth at the end of the collective pitch ramp
θ_s	Collective pitch and the end of ramp
C_T	Instantaneous thrust coefficient
$C_{T,s}$	Steady state thrust coefficient
λ	Instantaneous inflow velocity
λ_s	Steady state inflow velocity
N_b	Number of rotor blades
R	Rotor radius
c	Airfoil chord

Presented at the 64th Annual Forum of the American Helicopter Society, Montreal, Canada, April 29 – May 1 2008.

Introduction

Over the past decade, enhancements in computational fluid dynamic (CFD) methods, and the coupling of such methods to detailed and accurate models for the structural dynamics of the rotor, has led to significantly improved predictions of the detailed blade loads and resultant performance of rotorcraft in steady level flight (e.g. Refs. 1, 2). Simulations of rotorcraft performance in transient and maneuvering flight (Refs. 3, 4) have yet to meet with the same level of success, however. Predicting rotor performance under unsteady flight conditions is an extremely challenging problem, due in major part to the highly three dimensional and unsteady nature of the wake. A basic and fundamental understanding of the flow physics under such conditions remains elusive, yet is critical to the development of modeling tools that can be used successfully to predict the airloads and performance of helicopters during maneuvers.

Low order aerodynamic models (such as dy-

namic inflow models, indicial methods, quasi 2D stall models etc.) are routinely used in comprehensive rotorcraft codes because of the the high cost associated with higher fidelity approximations (such as full solutions of the unsteady Euler or Reynolds Averaged Navier–Stokes equations). Undeniably, these low-order models provide critical and useful information when they are integrated into the design cycle. It is well known though that such models have distinct limitations where rapid load changes, complicated wake interactions and flow separations become important factors in the aerodynamic behavior of the system. The present work examines the relative performance of three commonly-used aerodynamic formalisms with rather different inherent modeling fidelity. This is done by contrasting their performance in capturing the aerodynamic behaviour of a simplified, but highly unsteady, model rotor problem.

In an era of ever larger and more complex computations and experiments, the basic reductionist principle of the Scientific Method seems often to be forgotten. The value of a structured comparison of experiment and computation under carefully controlled, but simplified conditions, in being able to provide reliable information that is unambiguous and detailed enough to lead to an improved understanding of the flow physics, seems often to be underestimated in its potential to highlight the strengths and deficiencies of any particular modeling approach. The 1948 experiment of Carpenter and Fridovich (Ref. 5) is a good example of an investigation where some of the complex aerodynamic mechanisms that are relevant to non-steady rotor flight were captured within a very simple context. In that work, the response of a hovering helicopter rotor (in reality, a rotor mounted on a whirltower) to a ramp change in collective pitch was investigated experimentally and successfully compared to simple theory.

This experiment serves as an ideal reference for the present study because of the fundamental nature of the aerodynamic processes involved - the unsteady blade motion generates a complex, time-dependent pattern of shed and trailed vorticity in the wake of the rotor that has a profound effect on its loading. In the original experiment, however, the uncertainties associated with blade flexibility, variable rotor speeds, and also the rather complex geometry of the blades, hindered identification and characterization of all of the relevant flow phenomena.

In this work, Carpenter and Fridovich's experiment is replicated computationally, but the aerodynamics of the rotor is isolated from the structural dynamics of the blades and a very simple planform is substituted for the original blade geometry. This simplification allows a causal link to be established between the evolution of the wake and the associated build-up of inflow through the rotor, the dynamics of any flow separation on the blades, and the resultant thrust response of the rotor. The response of the rotor to a range of forcing conditions is simulated using varying levels of fluid dynamic approximation. Specifically, solutions obtained using a Compressible Reynolds Averaged Navier–Stokes approach are compared to results obtained from lifting-line theory coupled to an Eulerian Vorticity Transport Model, and from a simple single-state Dynamic Inflow model. The comparison offers some insight into the fundamental fluid dynamic mechanisms that govern the transient aerodynamic response of a rotor to control inputs, and provides some quantification of the limits of applicability of some popular current approaches to rotor aerodynamic analysis.

Details of test case

In the experimental investigations of Carpenter and Fridovich (Ref. 5), a three-bladed rotor, articulated both in flap and in lag, was attached to a whirl tower and subjected to various rates of ramp-input to the collective pitch of its blades. For rapid rates of collective pitch input, a large thrust overshoot was observed together with significant transient flapping of the rotor blades. The thrust overshoot was predicted to within 10% accuracy using a very simple, single state dynamic model for the inflow through the rotor. This test case has been simulated in the past, perhaps most notably by Bhagwat and Leishman (Ref. 6) who used a vortex filament representation of the wake to show that the rotor aerodynamic response is dominated by the circulatory field that is induced by the developing wake - and not by the inertia (or apparent mass) of the fluid in the wake as had been assumed by Carpenter and Fridovich in the derivation of their original dynamic inflow model.

In the present investigation, the experiment of Carpenter and Fridovich is replicated, but the two-bladed rotor of Caradonna and Tung (Ref. 13) is simulated rather than the rather complex blade geometry of the original experiment. This specific rotor was chosen because of its simple geometry and also because reliable steady state data for its hover performance is available, allowing the performance of the codes used to simulate the performance of the system to be verified under steady state conditions. The simulated rotor thus has a symmetrical NACA 0012 airfoil section, an untwisted rectangular planform, an aspect ratio of 6, and is operated at a tip Mach number of 0.439 and a tip Reynolds number of 1.92×10^6. The blades were assumed to be inflexible and to be rigidly attached to the rotor hub, thus decoupling the aerodynamic response of

the system from its structural dynamics.

In all simulations, the rotor was started at zero collective pitch, in which condition it generates zero lift. The collective pitch θ of the blades was then increased linearly[1] to reach a value $\theta = \theta_s$ after the rotor had turned through an azimuth angle $\psi = \psi_o$. The collective pitch was then kept constant at θ_s for the remainder of the simulation.

Computational methodology

Three computational approaches, with differing levels of physical representation of the aerodynamics of the rotor system, were used to simulate the aerodynamic behavior of the rotor in the simplified computational rendition of Carpenter and Fridovich's original experiment as described above.

1. Compressible RANS solver

CHRONoS (Compressible High Resolution Overset mesh Navier–StOkes Solver) is a vertex centered finite volume code for the solution of the Navier–Stokes equations on structured overset meshes. While the primary algorithm uses a hybrid RANS/LES coupling to represent the unresolved scales of the flow, in the present study the solver was employed in a fully turbulent RANS mode in which the Spalart-Allmaras turbulence model (Ref. 10) is integrated to the blade surface. The near-blade domain was discretized using a body-conforming mesh with dimension $229 \times 71 \times 67$ cells in the chordwise, spanwise and normal directions, respectively. This mesh was then overset inside a half-cylindrical background mesh with dimension $121 \times 91 \times 91$ cells in the azimuthal, vertical and radial directions, respectively. The azimuthal periodicity of the flow field of the two-bladed rotor system allowed the simulation to be performed on the mesh of a single blade together with its associated half-cylindrical background mesh. A hole with constant topology was cut in the rigidly rotating background mesh and local searches and interpolations were performed at every time-step to account for the motion of the blade mesh relative to the background mesh. A third-order Weighted Essentially Non-oscillatory scheme (Ref. 7), based on the AUSM-DV flux splitting method (Ref. 8) was used to discretize the inviscid terms. The viscous terms were computed using second order central differencing. Second order accurate implicit time integration was used with the Diagonalized Diagonally Dominant Alternating Direction Implicit scheme (Ref. 11). 2880 time steps per revolution

[1]For the RANS calculations, the pitch rate was made a continuous function by quadratically smoothing the start and end of the ramp-up phase.

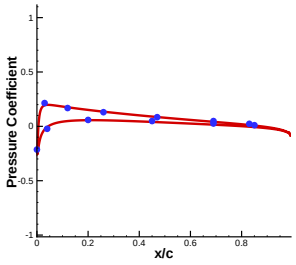

(a) $r/R = 0.5$

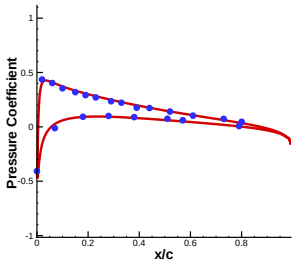

(b) $r/R = 0.68$

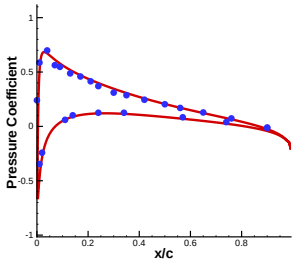

(c) $r/R = 0.8$

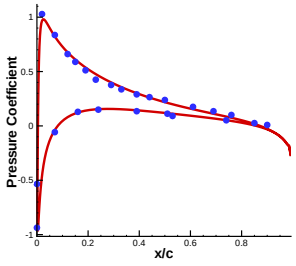

(d) $r/R = 0.96$

Figure 1: Comparison of RANS computed pressure coefficients with experiments at different spanwise sections for Caradonna and Tung's hovering rotor.

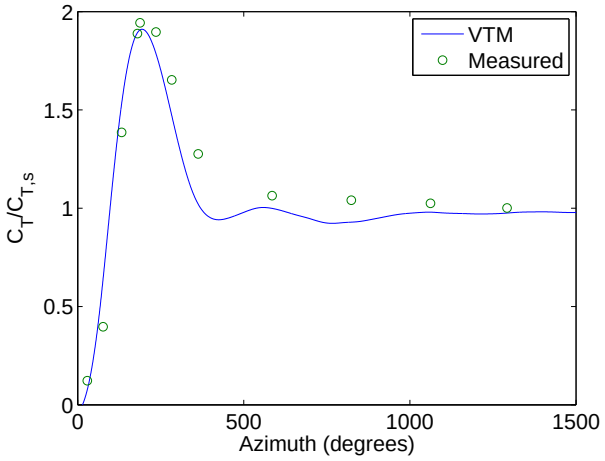

Figure 2: Comparison of VTM computed thrust response with experimentally measured values for a ramp change in collective pitch of a hovering rotor.

(with 10 to 20 sub-iterations per time step depending on the specific problem) were used to ensure time accuracy and convergence of the calculations.

As such, this methodology provides a consistent model for the evolution of the blade aerodynamics and the rotor wake that is based on a fundamental description of the fluid mechanics of the system. The approach is rendered specific to the configuration under study by specifying, in detail, the geometry of the rotor as the inner surface of the body-conforming grid and then applying suitable fluid boundary conditions on this surface. As such, the model should be inherently capable, at least as far as its innate description of the flow physics allows, of representing the various processes of lift generation, subsequent wake formation and eventual flow separation that are known to be important in the problem under consideration.

2. Lifting line model with Eulerian Vorticity Transport

A second approach used the Vorticity Transport Model (VTM) of Brown (Ref. 12) to capture the detailed evolution of the structure of the wake, in conjunction with a lifting-line approximation to the aerodynamics of the blades. The lifting-line model is based on the Weissinger-L formulation, in which the blade is discretized into a number of panels along its span. A bound vortex is attached to the quarter-chord of each panel; the strength of the vortex on each panel is determined by satisfying a condition of zero through-flow at a sequence of collocation points, located at the three-quarter chord, on all the panels simultaneously. The boundary condition at each collocation point is modified using a predictor-corrector approach to allow the sectional aerodynamic characteristics of the blade to match a pre-specified variation of lift coefficient with angle of attack. The resultant variation in loading along the length of the blade is translated into a vorticity source that is fed into the VTM wake model. The solution of the incompressible Navier–Stokes equations in vorticity - velocity form within the VTM allows for an accurate vorticity-preserving discretization of the convective terms on a relatively coarse mesh surrounding the rotor (in the present work, the size of the smallest cells within the computational domain was $R/55$). Explicit time marching was used throughout, with 350 time-steps per rotor revolution.

As such, the coupled lifting-line – VTM model represents the evolution of the wake in terms of a fundamental description of the fluid dynamics but approximates the flow physics near the blade. In particular, any representation of flow separation within the model is crucially dependent on the accuracy of the airfoil data that is used to generate the pre-specified variation of lift coefficient with angle of attack on each blade panel. This approach is quite commonly used in comprehensive rotor codes, but there are fundamental difficulties, for instance in incorporating the effects of strong three-dimensionality in the flow near the blade surface.

3. Single state dynamic inflow model

A third approach to modeling the simplified Carpenter and Fridovich problem used a variation on the dynamic inflow model that was developed in the original study (Ref. 5). In this approach, the average induced velocity through the rotor disc is represented as a single state within a simple first-order ordinary differential equation to model the delay in the response of the inflow through the rotor to a change in the thrust that is generated by the system.

This approach is commonly used in flight dynamic analyses to yield the aerodynamic loads on the helicopter rotors during transient flight conditions and maneuvers. In practice it is often necessary to expand considerably the number of states that is used to represent the variation of inflow across the rotor disc, but the approach is particularly attractive because its inherent formulation in terms of ordinary differential equations allows easy integration into analyses of helicopter stability and control. In the present context, the simplicity of the model allows an analytical solution to be derived for the variation in the thrust produced by the rotor in response to a ramp change in its collective pitch (see Appendix A). Although the approach is highly efficient if used properly, some aspects of the aerodynamics of the rotor system are poorly represented by the approach. For instance,

the formalism does not retain any representation whatsoever of the vortical structure of the rotor wake.

Model verification

Since a complete decoupling of the aerodynamic and structural characteristics of a real rotor system is not possible, validation of the predictions of the various approaches described above against experimental data that is directly relevant to the particular case that was modeled in this work is not feasible. The predictions of the various models are thus compared against a number of related experimental data sets in order to illustrate the basic validity of their approach.

Figure 1 shows a comparison between predictions obtained using CHRONoS and Caradonna and Tung's measurements (Ref. 13) of the chordwise variation of pressure coefficient at various stations along the span of their two-bladed, hovering rotor. The particular case presented in Fig. 1 is for a collective pitch of 8° and a tip Mach number of 0.439. The computations are seen to match well with the experimental data, and indeed the overall thrust computed for the rotor was found to be within 2% of the experimentally-measured value.

The predictions of the lifting-line - VTM model have also been compared with Caradonna and Tung's data and close agreement between the predicted and measured variation of loading along the span of the blades as well as of the vortical structure of the rotor wake has been obtained (Ref. 12). The predictive capabilities of this approach in the context of unsteady rotor aerodynamics are illustrated in Fig. 2. In this figure, VTM predictions of the variation of thrust with time are compared with the data obtained by Carpenter and Fridovich (Ref. 5) for their three-bladed rotor when subjected to a ramp change in collective pitch from 0° to 12° over roughly half a rotor revolution. The computed thrust response is seen to agree reasonably well with the measured data. Some of the discrepancies between experiment and prediction are thought to be directly attributable to errors in modeling the experimental system. For instance, the structural and inertial properties of the blades that were used in the experiment could not be determined fully from published information, and elastic torsion, although not modeled in the simulations, is very likely to have had a strong influence on the response of the rotor to sudden changes in its collective pitch.

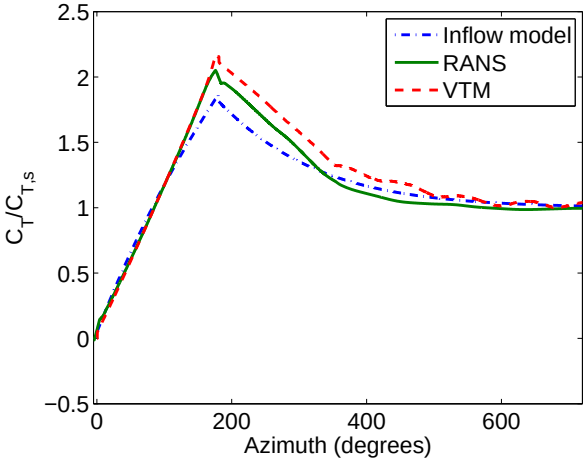

Figure 3: Variation of thrust coefficient with time for collective pitch ramped to 8° within an azimuth of 180° ($\theta_s = 8°, \psi_o = 180°$).

Results

Figure 3 shows the predicted evolution of the thrust coefficient (normalized by its steady value $C_{T,s}$) for the rigid, two-bladed rotor undergoing a ramp change in collective pitch from 0° to 8° over half a rotor revolution. An almost linear increase in thrust is observed during the pitch ramp. By the end of the ramp, the thrust is seen to have increased to 200% of its eventual steady-state value. As has been well documented (Ref. 6), this overshoot is attributed to the finite time that the wake takes to reach a steady state and the resultant lag in the development of the inflow through the rotor. After the ramp-up phase, the continued strengthening of the inflow yields a gradual decrease of thrust until a steady state is attained after approximately two rotor revolutions. The RANS and VTM predictions of the thrust response of the rotor agree well with each other. The dynamic inflow model yields a thrust response that matches reasonably well with the predictions of the other methods, although its predictions deviate subtly from the linear trend predicted by the other two methods during the pitch ramp.

Figure 4 compares the development of the sectional lift coefficient along the span of one of the rotor blades during the course of the first rotor revolution, as predicted by the RANS and VTM methods. The blade rotates in a counter-clockwise fashion. The predictions of the two models are in exceptionally good agreement. Starting from zero lift across the span, the lift distribution becomes heavily biased towards the tip of the blade by the end of the pitch ramp. Subsequently, as the downwash through the rotor evolves towards its steady state, the influence of the tip vortices drives the loading toward a more classical distribution where

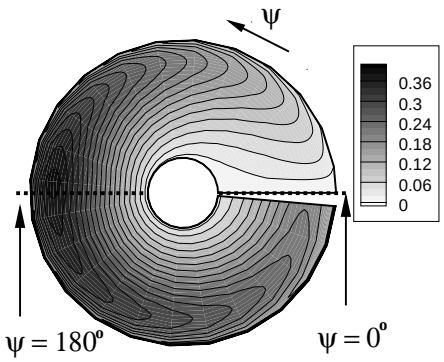

(a) RANS prediction

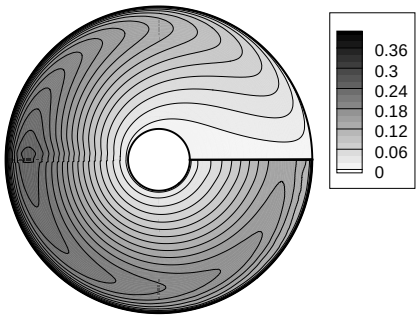

(b) VTM prediction

Figure 4: Variation of sectional lift coefficient along the span of the blade during the first rotor revolution ($\theta_s = 8°, \psi_o = 180°$).

the peak load is concentrated around the 75% radial station.

Figure 5 shows the predicted thrust response of the rotor when the pitch rate during the ramp-up phase is doubled while still retaining the same final collective pitch setting θ_s. In this case, all three models predict a linear increase in thrust during the ramp up phase. The thrust predicted by the RANS and VTM models is seen to increase for a short period after the end of the ramp-up phase before relaxing back to its eventual steady state. In strong contrast, the dynamic inflow model fails to capture the delay in the onset of the relaxation process and continues to predict the same monotonic decrease in thrust towards its eventual steady-state value following the end of the ramp-up phase that it does for lower pitch rates. This suggests that the RANS and VTM simulations are resolving physics that the dynamic inflow model is failing to represent. Figure 6 shows the rate of increase of sec-

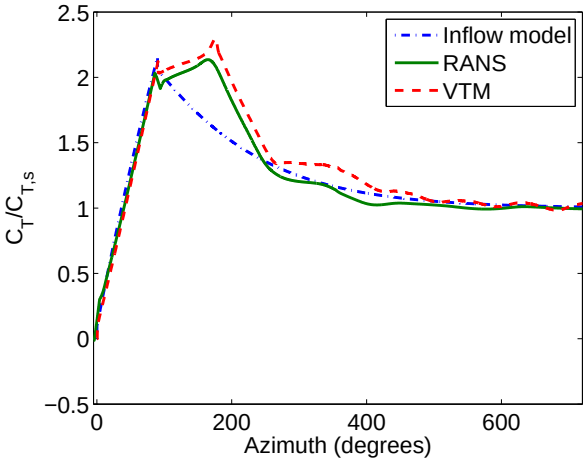

Figure 5: Variation of thrust coefficent with time for collective pitch ramped to 8° within an azimuth of 90° ($\theta_s = 8°, \psi_o = 90°$).

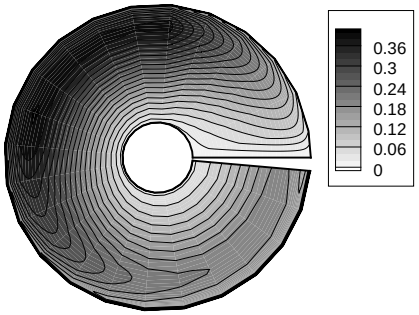

(a) RANS prediction

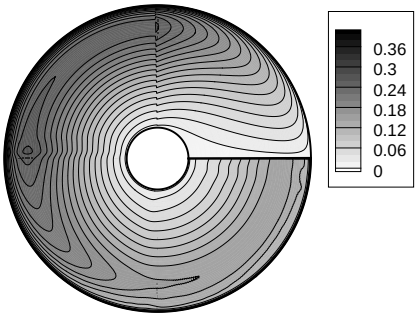

(b) VTM prediction

Figure 6: Variation of sectional lift coefficient along the span of the blade during the first rotor revolution ($\theta_s = 8°, \psi_o = 90°$).

tional lift coefficient along the span of the blade to be roughly uniform at all radial stations during the ramp-up phase, and, indeed, this to be the case until the blade reaches an azimuth of 180°. In the post ramp phase (i.e. for $\psi > 90°$ in this case), any thrust increase on the rotor (in the averaged sense) can only be explained in terms of a reduction in the mean inflow through the rotor. The relationship between thrust and inflow is clearly apparent if Fig. 5 is compared with Fig. 7(a), which shows the temporal variation of the inflow, averaged along the span of one of the blades, as predicted by the VTM and by the dynamic inflow model. As shown in Appendix A, the solutions to the single state dynamic inflow equation, assuming quasi-steady aerodynamics, are monotonic in time, and hence cannot represent the temporary reduction in inflow that occurs just after the cessation of the pitch ramp.

The origin of this reduction in inflow can be understood if one considers the response of an isolated airfoil to a ramp change in incidence. As is well known, the generation of lift by an airfoil under such circumstances is accompanied by vorticity being shed into the wake. This shed vorticity produces a downwash on the airfoil that reduces the lift that the airfoil experiences. At the end of the pitch ramp, in the absence of changes in incidence, the shed vorticity convects away from the trailing edge of the airfoil, its effect in inducing a downwash on the airfoil diminishes, and the lift produced by the airfoil gradually increases towards its final steady state (see Appendix B for a more complete analysis). The effect of this mechanism on the inflow experienced by the blades just post cessation of the ramp-up phase is clearly seen in the VTM predictions shown in Fig. 7(a).

The difference though between a two-bladed rotor subjected to a ramp pitch change and an airfoil subjected to a similar change in incidence is that, in the former case, the reduction in inflow is sustained only until $\psi = 180°$, after which each blade finds itself for the first time in the proximity of the tip vortex that was generated by the preceding blade. The starting vortex structure that is created by the preceding blade is generally quite diffuse for it not to play a primary role in this interaction[2]. The effect of this interaction on the load distribution along the rotor blades is clearly visible in Fig. 8. With the blade at 180°, the trailed vortex from the preceding blade induces a sudden change in the downwash distribution, especially near the blade tip, that marks the onset of the overall reduction in the thrust produced by the rotor.

It is very clear, thus, that there are *two* different relaxation time scales that govern the early stages of the thrust response of the rotor to a ramp change in its collective pitch. The first timescale is associated with the *reduction* of the induced velocity due to the blade's own *shed* vorticity following the end of the ramp-up phase. The second timescale is associated with a *delay* in the onset of the overall *increase* in induced velocity through the rotor because of the finite time taken for the blades to encounter the *trailed* vorticity from the preceding blades that is primarily responsible for this increase. It can easily be argued thus that this second timescale should be inversely proportional to the number of blades on the rotor. Indeed, Fig 9 shows how the aerodynamics on the two disparate timescales interact to produce the overall thrust response of the rotor for various different rates of increase of the collective pitch of its blades. The persistence of the break in aerodynamic behavior at $\psi = 180°$ for this two-bladed rotor, no matter what the rate of pitch increase, supports the essentially geometric origin of the second timescale.

The response of the rotor on the first timescale could be introduced into simpler representations of the aerodynamics of the rotor by using an indicial type approach to capture the unsteady aerodynamic response of the blade sections to changes in their incidence. This is routinely done in most comprehensive codes, in fact. The aerodynamic response on the second timescale will be missing though from any model that does not contain a representation of the detailed structure of the rotor wake and thus might prove quite difficult to incorporate in robust and rigorous fashion into the simplest models for the unsteady aerodynamic behavior of rotor systems.

Wake dynamics

To lend further insight into the discussion presented above, Fig. 10 shows the development of the vorticity distribution near the rotor, as predicted by the VTM. Each individual plot shows contours of vorticity magnitude on a vertical slice containing the rotor shaft. Figure 10(a) shows the shed and the trailed vortices to be located very slightly above the plane of the rotor disc during the first half-revolution of the rotor. Beyond this first half-revolution, the trailed vortices from the tips and roots of the two blades overlap to form a toroidal wake structure. As shown in Fig. 10(b), the toroid associated with the tip vorticity convects below the rotor disc under the influence of its self-induced velocity. The root toroid initially convects above the plane of the rotor before reversing direction after several rotor revolutions have elapsed. In a qualitative sense, the behavior of the outboard part of the rotor wake is representative of the flow field around

[2]Figure 7(b) does indeed show a small dipole-like perturbation to the loading along the length of the blade near $\psi = 180°$ that is caused by interaction with the starting vortex structure that is shed by the preceding blade during the pitch ramp.

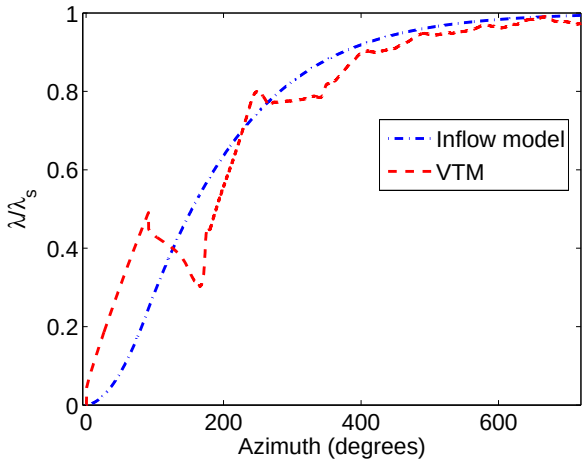

(a) $\theta_s = 8°, \psi_o = 90°$

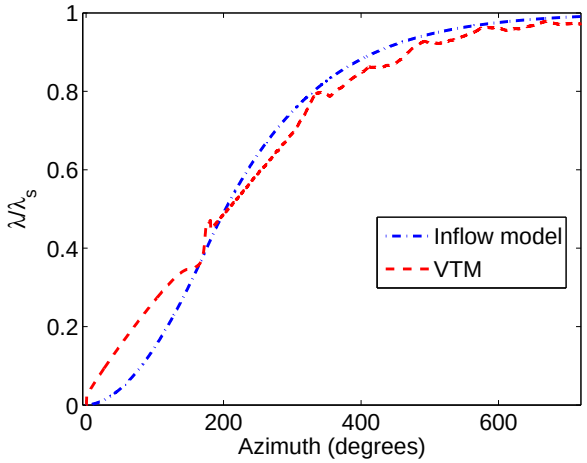

(b) $\theta_s = 8°, \psi_o = 180°$

Figure 7: Variation of inflow through the rotor disc with time as predicted by the VTM (averaged over the blade span) and the dynamic inflow model (averaged over the rotor disc).

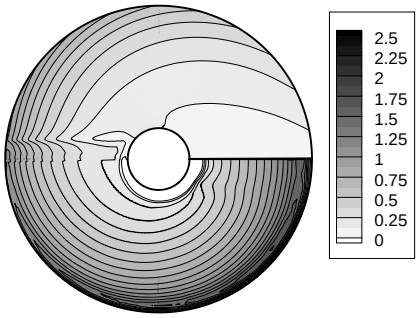

(a) $\theta_s = 8°, \psi_o = 180°$

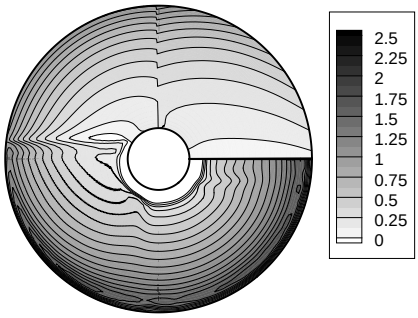

(b) $\theta_s = 8°, \psi_o = 90°$

Figure 8: Variation of inflow (non-dimensionalized by the final steady value) along the span of the blade during the first rotor revolution as predicted by the VTM.

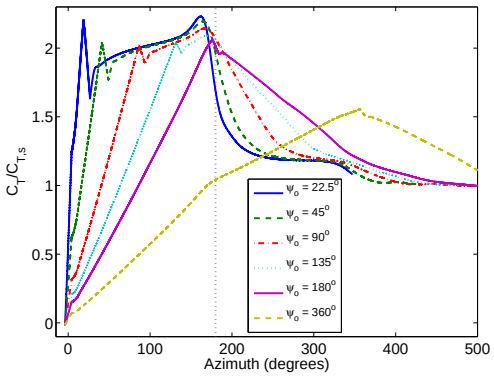

Figure 9: Variation of thrust coefficient with time as predicted by the RANS model for $\theta_s = 8°$ and various ψ_o.

an impervious disc that is impulsively accelerated along its axis. In the initial stages of the evolution of the wake, it can be argued thus that the theoretical framework of the dynamic inflow model in terms of the virtual mass of an accelerated region of fluid enclosing the rotor is justified, at least in a phenomenological sense.

At the very early stages in the evolution of the wake, it is thus not surprising that the quantitative predictions of the inflow model compare well with the predictions of the more physically-complete RANS and VTM models. Shortly after the first half-revolution of the rotor, though, the system enters a short-lived regime in which the interaction between the starting vortex from each of the blades and the evolving tip vortices results in a highly complex wake structure. Figures 10(c)-(d) show the starting vortices from the blades to be distorted significantly by their interaction with the toroidal tip-vortex structure, and eventually to be wrapped, in spiral fashion, around the core of the toroid. In this regime, accurate prediction of the detailed time dependence of the loading on the rotor is strongly reliant on accurate modelling of the structure of the rotor wake. Nevertheless, as the toroidal tip vortex structure continues to convect below the rotor under the influence of its own self-induced velocity (as shown in Fig. 10(e)-(f)), the newly generated tip vortices eventually organize themselves into the classical contracted wake configuration that is again amenable to analysis by the simpler models.

Operation in the Stalled regime

For the cases discussed thus far, the forcing conditions were such that the boundary layer remained attached to the blade surface throughout. Figure 11 shows the predicted thrust response of the rotor when the collective pitch setting θ_s at the end of the ramp-up phase is increased to 20°. With this value of θ_s, the flow separates from the surface of the blades at some point as the collective pitch is increased. During the ramp-up phase itself, the same good agreement between the predictions of the RANS model, VTM and inflow model as at lower values of θ_s is still observed. In fact, for all simulations that have been conducted with $4^\circ \leq \theta_s \leq 30^\circ$, the thrust response to collective pitch input has been found to be approximately linear during the ramp up phase. There is significant variation between the predictions of the three models in the post-ramp phase, however. While the inflow model does not account for flow separation, the RANS and VTM results are also in some disagreement; the RANS solutions show a more abrupt loss in thrust after the ramp-up phase and the relaxation to the steady value to be much

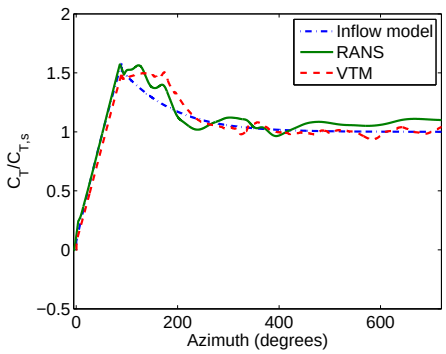

(a) $\psi_o = 90^o$

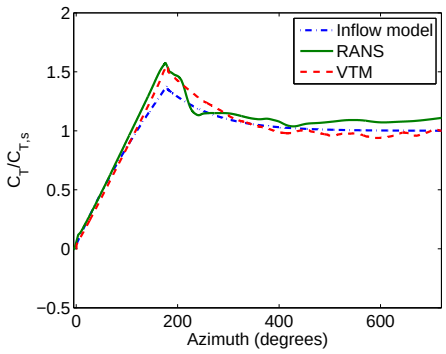

(b) $\psi_o = 180^o$

Figure 11: Variation of thrust coefficient with time for $\theta_s = 20^\circ$.

more gradual than predicted by the VTM. This appears to be because the additional non-linearity and three-dimensionality of the flow when regions of separated flow are present on the blade produces a far more unsteady variation of thrust on the rotor than when the flow remains unstalled. Indeed, comparing the thrust responses shown in Figs. 12(a) and (b) suggests that the unsteadiness in the thrust that is produced by the rotor in the post-ramp phase is strongly dependent on the rate of pitch increase during the ramp-up phase. The origin of this effect appears to be in the details of the vortex shedding process from the blade during the onset of separation and the resultant pattern of non-uniformities in the shed and trailed vorticity distribution that is created in the wake behind the rotor blades.

The thrust response of the rotor for various final pitch settings, as predicted by the RANS model, is compared in Fig. 12. In each case, the thrust produced by the rotor has been normalized by its eventual steady-state value. The onset of flow separation is seen to reduce significantly any post-ramp excursions in the thrust produced by the rotor. This is most likely due to a combination of two effects. Firstly, the increased convection rate of the wake vortices that are produced by the system at higher thrust results in their effect on the per-

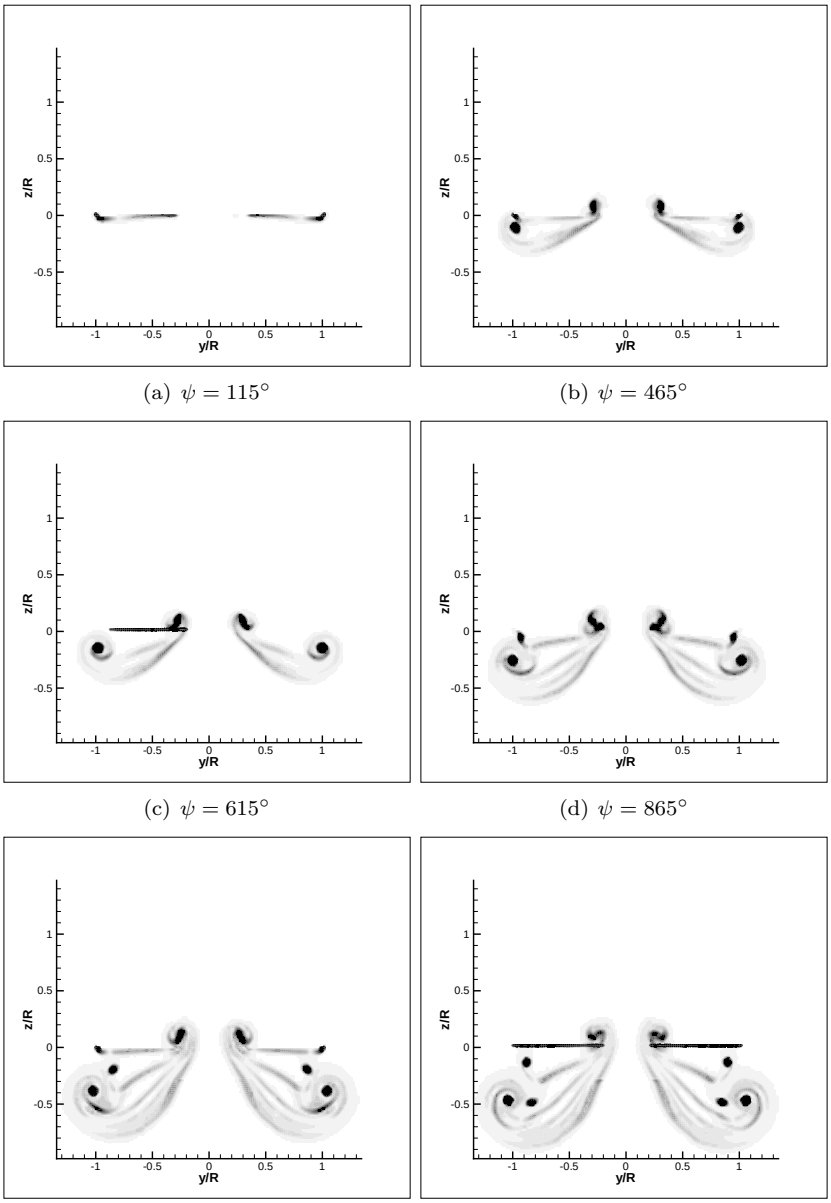

(a) $\psi = 115°$ (b) $\psi = 465°$

(c) $\psi = 615°$ (d) $\psi = 865°$

(e) $\psi = 1165°$ (f) $\psi = 1315°$

Figure 10: Contours of VTM computed wake vorticity magnitude for $\theta_s = 8°, \psi_o = 90°$, on a sectional plane positioned at $\psi = 90°$. Rotor disc plane is located at z=0.

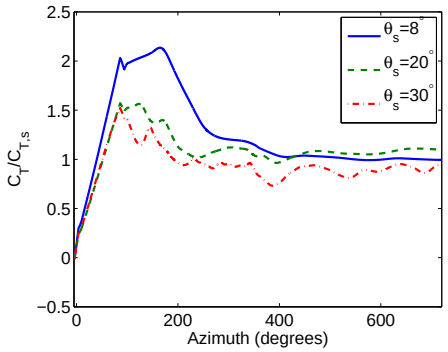

Figure 12: Variation of thrust coefficient with time for $\psi_o = 90°$ and various θ_s as predicted by the RANS model.

formance of the system being far more transient than at lower thrust. Secondly, the aerodynamic response of the blade sections to any change in the inflow that they experience as a result of the developing wake is known to be significantly curtailed in the presence of flow separation.

The formation and propagation of flow separation on the blades of the rotor is detailed in Figs. 13 and 14 for the case when $\theta_s = 20°$ and $\psi_o = 90°$. Figure 13 shows the extent of the reverse flow region on the upper surface of the blade, with the blade at various azimuthal locations. Evidence of initial separation is seen when the blade is near 65° azimuth. Figure 13(a) shows a leading edge separation bubble, concentrated at around 80% of the blade radius. Indeed, separation was seen to initiate at this radial location in all other stalled cases that were simulated. This localization may be attributed to the fact that the local effective angle of attack $\theta - \lambda/\Omega r$ is the largest at this radial location when the stall is initiated.

Figures 14(a) and 13(b) show the separation bubble to grow in size in both the chordwise and spanwise directions as the pitch of the blade is increased further. As the separated flow region grows in size, centrifugal and Coriolis forces take effect and a significant spanwise flow begins to develop along the length of the blade. Near the center of the separation bubble, the streamwise velocity component relative to the blade surface is very small. The centrifugal forces then induce a spanwise flow. The resultant Coriolis effect then forces the core of the separation bubble to trace a curved path relative to the blade surface as shown in Fig. 14(b). The flow topology is extremely complicated in that there are two distinct regions of flow separation above the blade surface. Figures 13(c) and (d) show a separation bubble over the entire span of the blade near its leading edge together with a secondary region of flow separation that results from the spanwise convection of a stall vortex that is initiated at the leading edge of the blade root.

The tip vortex plays a critical role throughout the development of the stalled flow on the blade surface. The strong velocities that it induces on the surface of the blade ensures that the tip region remains free of stall. In addition, it is clearly apparent from Fig. 14 that the vortical structures associated with the inboard flow separation are able to persist for a long period of time over the blade surface. The stability of these flow structures is maintained by a process whereby their vorticity, which is primarily oriented along the span of the blades, is 'drained' into the tip vortex. Figures 13(c) and 14(e) show almost all of the flow over the blade surface to have separated in this particular case once the blade has rotated to 270° azimuth. Eventually, the continued strengthening of the inflow through the rotor that accompanies the development of its wake causes the flow to re-attach over a large portion of the blade surface, as is shown in Figs. 13(d) and 14(f).

Although the predictions of the RANS method still need to be treated with some care given the likely dependence of the detailed behavior of the system on the formulation of the turbulence model and so on, a good qualitative representation of the physics can be expected in situations such as that presented here for the simple reason that the the kinematics of the flow structures play a dominant role in the evolution of the flow separation. Indeed, it is very clear from the RANS simulations that the propagation of the separated flow regions across the blade surface is a highly three dimensional process. This characteristic of the fluid dynamics is very poorly represented by the lifting-line model used to generate the blade loads within the VTM simulations and is largely responsible for the observed discrepancies between the predictions of the two approaches in this case. Despite the popularity within the rotorcraft community of several ad-hoc 'fixes' to lifting-line theory to account for the three-dimensional character of flow separation along the blades of a lifting rotor, it is likely that rigorous and robust incorporation of some of the fluid physics revealed in this section into the lifting-line formalism will prove to be an extremely challenging task, if at all possible.

Summary and Conclusions

Although much success has been achieved in modeling the aerodynamic behavior of helicopter rotors in steady flight, similar analyses of rotor performance under transient or maneuvering conditions still prove to be problematic. This is largely because of the highly transient and three-dimensional character of the rotor wake, and the resultant complexity of its aerodynamic interaction with the rotor itself, in such circumstances.

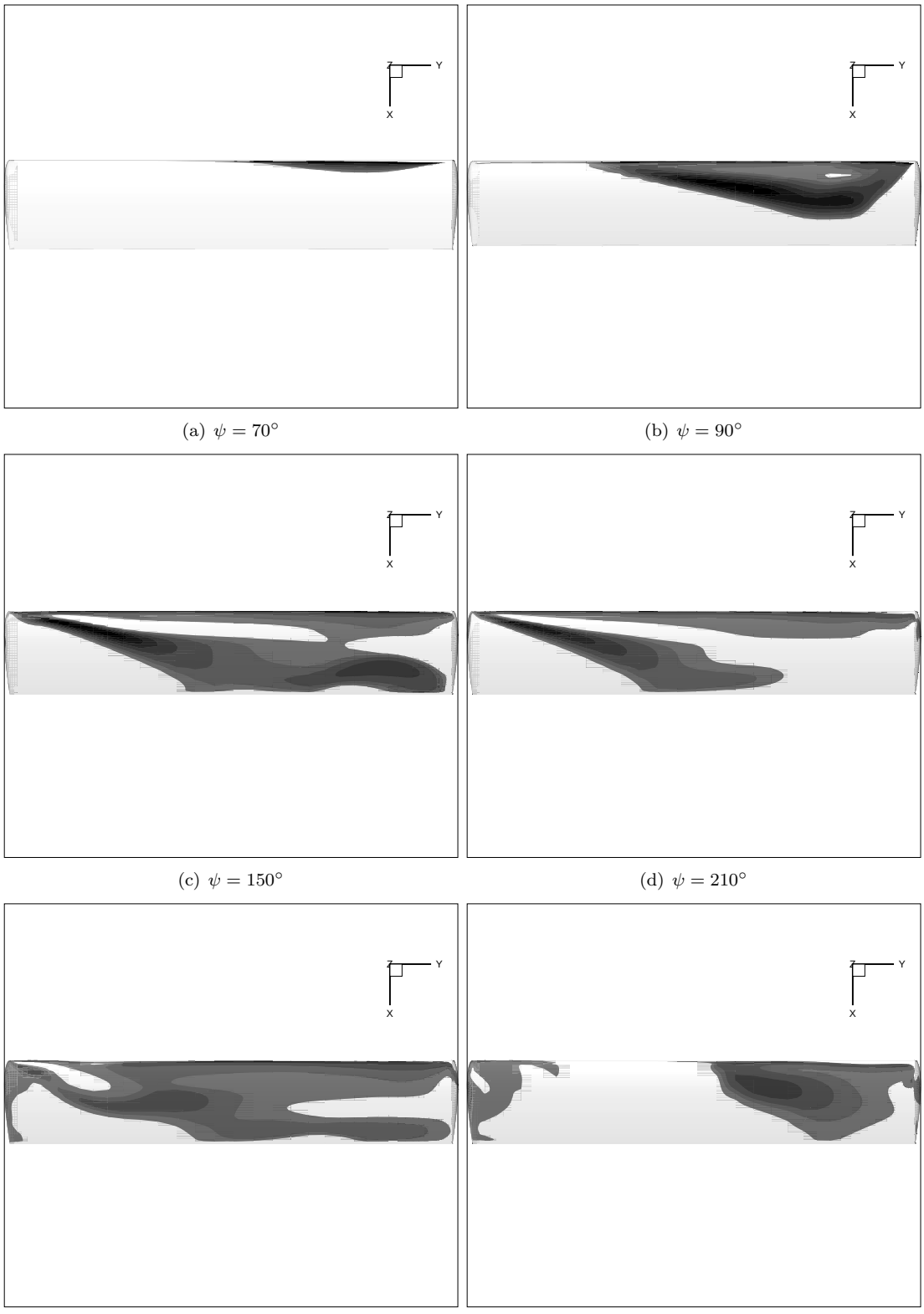

(a) $\psi = 70°$ (b) $\psi = 90°$

(c) $\psi = 150°$ (d) $\psi = 210°$

(e) $\psi = 270°$ (f) $\psi = 360°$

Figure 13: Flow separation regions on top surface of the blade as predicted by the RANS model ($\theta_s = 30°, \psi_o = 90°$).

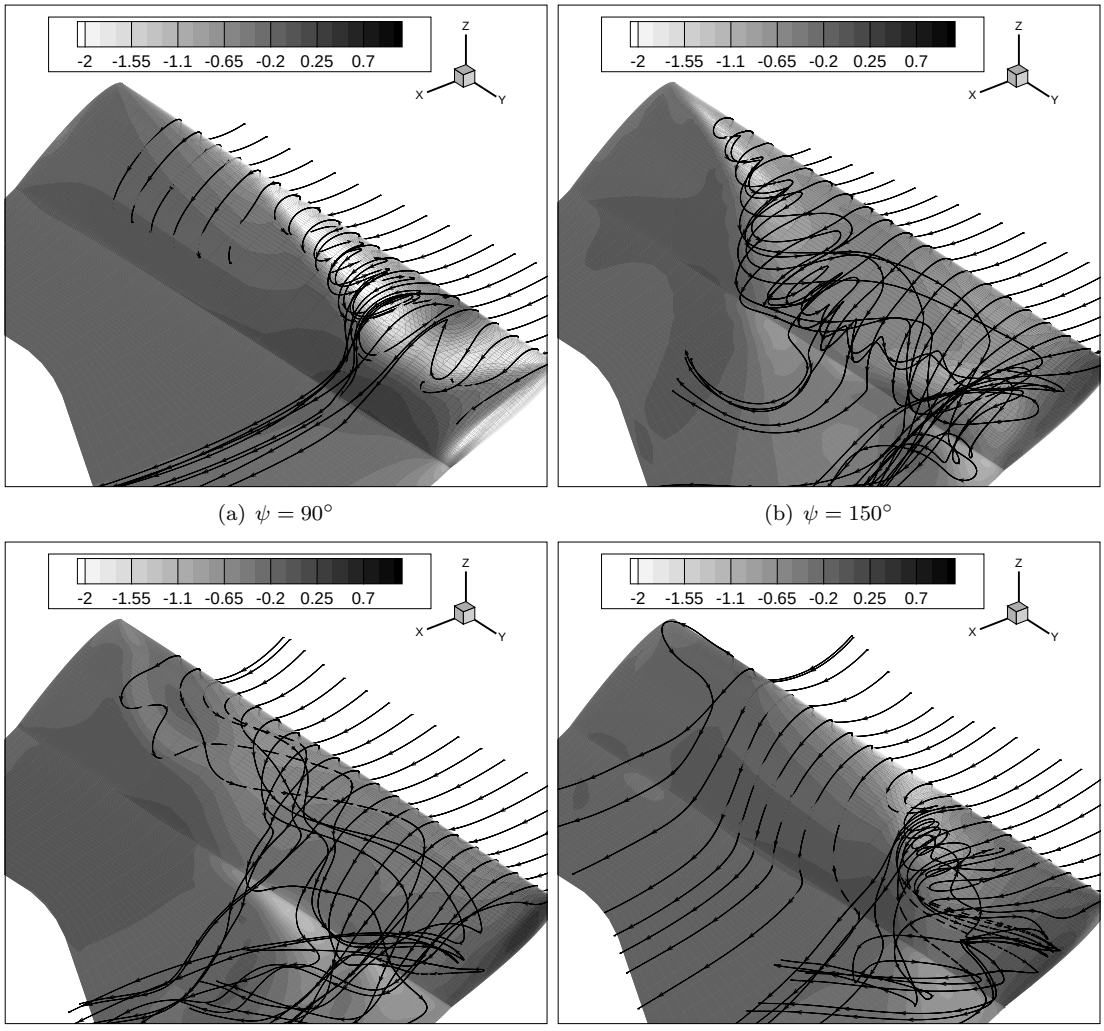

(a) $\psi = 90^\circ$ (b) $\psi = 150^\circ$

(c) $\psi = 270^\circ$ (d) $\psi = 360^\circ$

Figure 14: Streamlines in the flow near the blade during flow separation as predicted by the RANS model, superimposed on top of pressure coefficient contours ($\theta_s = 20^\circ, \psi_o = 90^\circ$).

To lend some insight into the principal fluid dynamic mechanisms that are at work near the blades and in the wake of a helicopter rotor in such situations, the response of a simple, two-bladed hovering rotor to a ramp change in collective pitch was simulated using three computational approaches that are typical of current practice. Solutions obtained using a Compressible Reynolds Averaged Navier–Stokes (RANS) approach were compared to results obtained from lifting-line theory coupled to an Eulerian Vorticity Transport Model (VTM), and from a simple single-state dynamic inflow model.

The RANS model is capable of representing, from first principles, the various processes of lift generation, subsequent wake formation and eventual flow separation that are known to be important in the problem under consideration. This is despite the fact that detailed predictions using the approach, particularly in the separated flow regime, are to some extent influenced by modelling assumptions – most notably by the approach taken to incorporating the effects of turbulence within the flow system.

In comparison, the lifting-line model in conjunction with the VTM provides a first-principles description of the dynamics of the wake, but approximates the aerodynamics of the blade, particularly in the post-stall regime, in terms of prescribed two-dimensional airfoil characteristics.

The single-state dynamic inflow model that was used in the present work relies on a modification to standard momentum theory to capture the gross effects of the delay in response of the inflow through the rotor to any change in loading on the system. It provides a very simple phenomenological model for the aerodynamic environment of the rotor that is similar to the approach that is often used in the flight dynamics community because of its advantageous mathematical structure. The model does not embody any representation of the vortical structure of the wake, however.

The three different numerical approaches yield very similar predictions of the thrust response of the rotor to ramp changes in collective pitch, as long as these pitch changes are slow enough to extend over a significant part of a single rotor revolution. This suggests that the basic underlying fluid dynamic mechanism, whereby a delay in the establishment of the inflow through the rotor is responsible for an associated overshoot in the thrust produced by the system, is properly represented by all the approaches. Detailed analysis of the development of the wake and the associated variation of the inflow that is experienced by the blades of the rotor supports earlier findings that this delay results from the finite time that it takes for the toroidal starting structure that is produced during the first rotor revolution to propagate away from the rotor and for the wake to establish the tubular, heliocoidal structure that is characteristic of its steady state.

Tests involving more rapid ramp rates reveal additional detail within the wake as the inflow builds to its steady-state value. The initial thrust response of the rotor in the post-ramp phase is dominated by two different physical processes with different associated time scales. The interaction of each blade with its own shed vortex results in a slow increase in loading on the system as this structure is left behind in the wake. This process is well represented by both the VTM and RANS models, and could quite feasibly be captured in the dynamic inflow formalism by using an indicial model to represent the unsteady aerodynamic behavior of the airfoil sections. Although the interaction of each blade with the trailed vorticity that is produced by the remainder of the system has been known for some time to be the fundamental mechanism by which the inflow experienced by the blades increases over time, a delay in the onset of this mechanism because of the finite extent of the trailing vortex during the early history of the rotor wake does not seem to have been noticed previously. The duration of this delay appears to be related directly to the rotation speed and number of blades of the rotor. Nonetheless, incorporation of this effect into simulations would be fundamentally reliant on the model containing a representation of the detailed structure of the rotor wake. Arguably, though, the effect could be included in the dynamic inflow formalism via a simple ad-hoc modification.

Even though the evolution of the wake of the rotor is strongly three dimensional and highly unsteady, the predictions of the Reynolds Averaged Navier–Stokes and VTM - lifting-line models agree very closely as long as the blades of the rotor do not stall. This suggests that in the pre-stall regime, a quasi two-dimensional representation of the blade aerodynamics is adequate for predicting the performance of such systems, as long as the circulatory feedback from the wake is accounted for. When flow separation occurs, three dimensional aerodynamic effects near the blade surface become important and the predictions of the Reynolds Averaged Navier–Stokes and lifting-line approaches begin to diverge quite considerably. The RANS calculations show the post-stall aerodynamic environment near the surface of the blade to be dominated by a highly complex interaction between a powerful vortical structure that sweeps along the top surface of the blade, and the trailed vortex that is produced at the tip of the blade. It is highly unlikely that the effects on blade loading of features such as these could be incorporated with any degree of rigor into simpler models for the aerodynamics of the rotor system.

The characterization of the wake interactions and stall propagation mechanisms that are presented in this study offers some insight into the fundamental fluid dynamic mechanisms that govern the transient aerodynamic response of a rotor to control inputs, and provides some quantification of the limits of applicability of some popular current approaches to rotor aerodynamic modeling in the analysis of the performance of rotor systems under unsteady conditions.

Acknowledgments

The authors would like to thank Vinit Gupta (Metacomp Technologies Inc.) for creating the parallel framework for CHRONoS and and Mr. Hariswaran Sitaraman (Indian Institute of Technology, Madras) for the development of the library routines used in dynamic overset mesh connectivity. The authors would also like to thank Adam Kenyon, Hyo Won Kim and Timothy Fletcher for generating the numerical results presented in Fig. 2.

Appendix

A. Exact solution to the single state dynamic inflow model

The dynamic inflow model of Carpenter and Fridovich (Ref. 5) relates the instantaneous, disc-averaged inflow velocity λ to the thrust produced by the rotor via the first-order ordinary differential equation

$$m\frac{d\lambda}{dt} + 2\pi R^2 \rho \lambda^2 = T \tag{1}$$

In this expression, $m = 0.637 \times \frac{4}{3}\pi\rho R^3$ is an apparent mass term, derived by assuming the rotor to be an impervious accelerating disc in an inviscid, incompressible fluid. For the present problem, lengths are non-dimensionalized by the rotor radius and the air density ρ is set to unity. For untwisted, untapered blades of chord c and an airfoil with a lift curve slope $C_{l\alpha}$, quasi-steady linear aerodynamics leads to the relationship[3]

$$m\frac{d\lambda}{dt} + 2\pi\lambda^2 + \frac{N_b C_{l\alpha} c}{4}\lambda = \frac{N_b C_{l\alpha} c}{6}\theta(t) \tag{2}$$

where the forcing $\theta(t)$ is the instantaneous collective pitch applied to the rotor. For the present application, a ramp change in pitch from $\theta = 0$ to θ_s over time $t = 0$ to $t = t_o$ is assumed so that

$$\theta(t) = \theta_s \frac{t}{t_o} = \dot{\theta} t \;\text{ if }\; t < t_o \tag{3}$$

$$\theta(t) = \theta_s \;\text{ if }\; t > t_o \tag{4}$$

Equation 2 can be solved numerically using any standard technique for ordinary differential equations. An exact solution can also be derived, however[4]. The exact solution is derived in two steps.

First, the inner solution of the ODE, valid for $0 \le t \le t_o$, is determined. This is done by recognizing that the ODE is a non-linear Riccati-type equation (Ref. 14) with linear forcing and thus can be solved by transforming to an equivalent linear equation once a particular solution is found. The inner solution (in terms of Airy functions (Ref. 15) Ai and Bi and their derivatives Ai' and Bi') is given by

$$\lambda_i(t) = C_1 \left[C_2 \left(\frac{C_3 Ai'(k(t)) + Bi'(k(t))}{C_3 Ai(k(t)) + Bi(k(t))} \right) - 1 \right] \tag{5}$$

Once the inner solution is obtained, the outer solution, valid for $t_o \le t \le \infty$, is determined by using $\lambda_i(t_o)$ as the initial condition for a second Riccati equation with constant forcing. The solution to this equation has exponential behaviour and is given by

$$\lambda_o(t) = C_4 + \frac{1}{-\frac{2\pi}{mC_5} + C_6 e^{C_5 t}} \tag{6}$$

In the equations given above, $k(t)$ is a linear function of time and C_i and d_i are constants given by

$$\begin{aligned}
k(t) &= \frac{d_2^2 + 4d_3^3 t}{4d_3^2} \\
C_1 &= \frac{d_1 \dot{\theta}}{12m} \\
C_2 &= 2\frac{d_3}{d_2} \\
C_3 &= \frac{2d_3 Bi'(k(0)) - d_2 Bi(k(0))}{d_2 Ai(k(0)) - 2d_3 Ai'(k(0))} \\
C_4 &= \frac{-d_2 + \sqrt{d_2^2 + \frac{4\pi d_1 \theta_s}{3m^2}}}{\frac{4\pi}{m}} \\
C_5 &= d_2 + \frac{4C_4\pi}{m} \\
C_6 &= e^{-C_5 t_o}\left[\frac{1}{\lambda_i(t_o) - C_4} + \frac{2\pi}{mC_5}\right] \\
d_1 &= N_b C_{l\alpha} c \\
d_2 &= \frac{d_1}{4m} \\
d_3 &= \left[\frac{\pi d_1 \dot{\theta}}{3m^2}\right]^{\frac{1}{3}}
\end{aligned}$$

[3] As mentioned in Ref. 5, a correction term can be added to reduce the error in averaging the inflow over the rotor disc. The effect of this term as confirmed by numerical solution, is actually minor and its exclusion does not change the qualitative behaviour of the solution

[4] Such a solution does not appear to have been published previously.

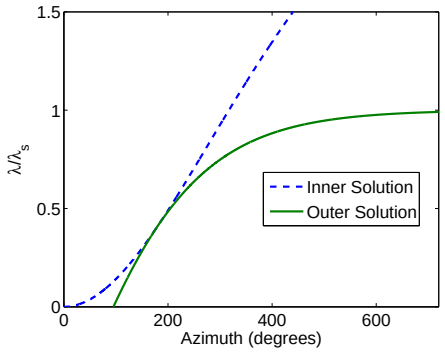

Figure 15: Inner (pre-ramp) and outer (post-ramp) exact solutions for a sample case with $\theta_s = 8°$, $\psi_o = 180°$.

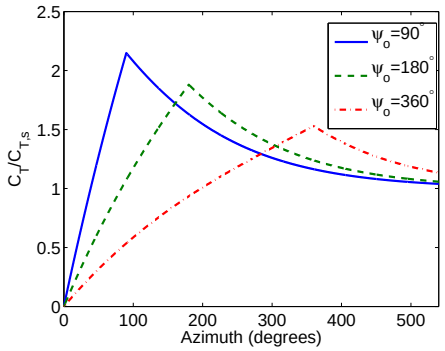

Figure 16: Exact solution for $\theta_s = 8°$.

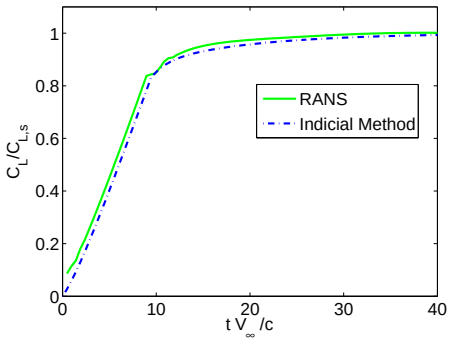

(a) Lift Coefficient

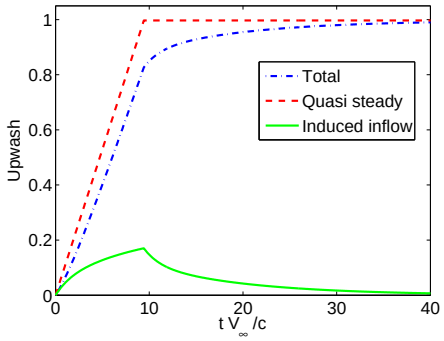

(b) Inflow (Indicial method)

Figure 17: Response of a NACA 0012 airfoil to a ramp change in pitch input.

Note that lengths and velocities have been nondimensionalized by the rotor radius and the tip speed, respectively. Figure 15 shows the solution for a typical case. The inner and outer solutions both increase monotonically with time. Although the aerodynamics of the blades has been assumed to be linear, Fig. 16 shows the thrust response of the rotor during the ramping phase to deviates quite significantly from linearity for larger azimuth angles.

B. Lift response of an airfoil to a ramp change in pitch

In order to understand the 2D aerodynamic mechanisms that affect the blade aerodynamics in the current problem, the response of an isolated airfoil to a ramp change in pitch input is presented here. Assume the same NACA 0012 airfoil as used on the rotor to be placed in a freestream at the same Mach number M=0.439 as the tip of the rotor. The airfoil is then subjected to a ramp change in its incidence, $\alpha(t)$, from 0° to 8° within a non dimensional time $t_o^* = 9.42$, after which the incidence is held constant. This time corresponds to 9.42 chord lengths of freestream traverse which is equal to the distance that is traveled by the tip of the rotor in rotating through an azimuth of 90°. The resultant variation in lift with time, as predicted by the CHRONoS RANS solver, is compared in Fig. 17(a) to the predictions of a standard indicial model (Ref. 9). The lift is seen to increase almost linearly until the end of the ramp phase, after which it asymptotes to its eventual steady value at a slower rate as the shed vorticity produced at the blade trailing edge convects downstream. The indicial model captures very well the behavior that is predicted by the RANS model; pitch rate terms and an apparent mass contribution could quite feasibly be added to further improve its predictions. Figure 18 compares the induced velocities at the airfoil that are produced by different ramp rates. It is worth noting how slowly the induced velocity decays in the post ramp phase compared to the rapidity of its development while the incidence of the airfoil is being varied.

References

[1]Datta, A., Nixon, M., and Chopra, I., "Rotor Loads Prediction with the Emergence of Rotorcraft CFD," 31st European Rotorcraft Forum, Florence, Italy, September 2005.

[2]Sitaraman, J., Datta, A., Baeder, J., and Chopra, I., "CFD/CSD Coupling for Aerodynamic

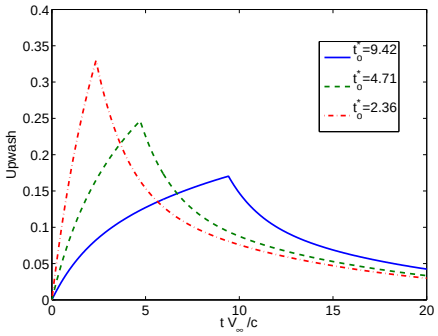

Figure 18: Induced inflow response of a thin airfoil subject to different ramp rates of change in pitch input.

and Structural Loads at three Critical Flight Conditions," 31st European Rotorcraft Forum, Florence, Italy, September 2005.

[3]Bhagwat, M., Ormiston, A., Saberi, H., and Xin, H., "Application of CFD/CSD Coupling for Analysis of Rotorcraft Airloads and Blade Loads in Maneuvering Flight," 63rd Annual Forum of the American Helicopter Society, Virginia Beach, Virginia, May 2007.

[4]Abishek, A., Datta, A., and Chopra, I., "Comprehensive Analysis, Prediction, and Validation of UH-60A Blade Loads in Unsteady Maneuvering Flight," 63rd Annual Forum of the American Helicopter Society, Virginia Beach, Virginia, May 2007.

[5]Carpenter, P., and Fridovich, B., "Effect of a Rapid Blade-Pitch Increase on the Thrust and Induced-velocity Response of a Full-scale Helicopter Rotor," *NACA TN 3044*, 1953.

[6]Bhagwat, M., and Leishman, G., "Transient Rotor Inflow Using a Time-Accurate Free-Vortex Wake Model," AIAA Paper 2001-0993, 39th AIAA Aerospace Sciences Meeting, Reno, NV, 2001.

[7]Liu, X., Osher, S., and Chan, T., "Weighted Essentially Non-oscillatory Schemes," *Journal of Computational Physics*, 115, (1994).

[8]Wada, Y., and Liou, M., "An Accurate and Robust Flux Splitting Scheme for Shock and Contact Discontinuities," *SIAM Journal of Scientific Computing*, 18 (3), pp. 633-657, 1997.

[9]Leishman, G., *Principles of Helicopter Aerodynamics*, Cambridge University Press, 2001.

[10]Spalart, P., and Allmaras, S., "A One-equation Turbulence Model for Aerodynamic Flows," 30th AIAA Aerospace Sciences Meeting, Reno, NV, January 1992.

[11]Klopfer, G., Hung, C., Van der Wijngaart, R., and Onufer, J., "A Diagonalized Diagonal Dominant Alternating Direction Implicit (D3ADI) Scheme and Subiteration Correction," AIAA-98-2824, 29th AIAA Fluid Dynamics Conference, Albuquerque, NM, June 1998.

[12]Brown, R., and Line, A., "Efficient High-Resolution Wake Modeling using the Vorticity Transport Equation," *AIAA Journal*, Vol. 43 (7), 2005.

[13]Caradonna, F.X. and Tung, C., "Experimental and Analytical Studies of a Model Helicopter Rotor in Hover," *NASA TM 81232,* 1981.

[14]Ince, E. L., *Ordinary Differential Equations*, Dover Publications, New York, pp. 23–25, 1956.

[15]Abramovitz, M., and Stegun, I., *Handbook of Mathematical Functions*, Dover Publications, New York, pp. 446, 1994.